



Ambient template synthesis of multiferroic MnWO_4 nanowires and nanowire arrays

Hongjun Zhou^a, Yuen Yiu^b, M.C. Aronson^{b,c}, Stanislaus S. Wong^{a,c,*}

^a Department of Chemistry, State University of New York at Stony Brook, Stony Brook, NY 11794-3400, USA

^b Department of Physics, State University of New York at Stony Brook, Stony Brook, NY 11794-3400, USA

^c Condensed Matter Physics and Materials Sciences Department, Brookhaven National Laboratory, Upton, NY 11973, USA

ARTICLE INFO

Article history:

Received 17 January 2008

Received in revised form

17 March 2008

Accepted 18 March 2008

Available online 21 March 2008

Keywords:

Magnetic properties

Nanowires

Multiferroic materials

ABSTRACT

The current report describes the systematic synthesis of polycrystalline, multiferroic MnWO_4 nanowires and nanowire arrays with controllable chemical composition and morphology, using a modified template-directed methodology under ambient room-temperature conditions. We were able to synthesize nanowires measuring 55 ± 10 , 100 ± 20 , and 260 ± 40 nm in diameter, respectively, with lengths ranging in the microns. Extensive characterization of as-prepared samples has been performed using X-ray diffraction, scanning electron microscopy, transmission electron microscopy (TEM), high-resolution TEM, and energy-dispersive X-ray spectroscopy. Magnetic behavior in these systems was also probed.

© 2008 Elsevier Inc. All rights reserved.

1. Introduction

Multiferroic materials [1,2], which show simultaneous ferromagnetic ordering (or any other kind of magnetic) and ferroelectric ordering, have attracted a lot of attention because of the coupling between the magnetic and dielectric properties in these systems as well as their control by application of magnetic and/or electric fields. A number of multiferroic transition metal oxide materials exist including BiFeO_3 [3], BiMnO_3 [4], TbMnO_3 [2], and DyMnO_3 [5]. A characteristic property of many of these materials is the simultaneous occurrence of a ferroelectric phase transition as well as a magnetic one, suggesting a strong interplay between the magnetic and ferroelectric order in these systems and implying that these materials hold particular promise in applications as diverse as information storage, spintronics, and sensors.

MnWO_4 , otherwise known as hübnerite, is a relatively lesser-known member of this class of materials and possesses spontaneous electric polarization manifested in a spiral magnetically ordered state [6–10]. MnWO_4 belongs to the monoclinic $P2/c$ space group, characterized by alternating layers of transition-metal and tungsten atoms parallel to the (100) plane, as shown in Fig. S1 [10,11]. Specifically, each Mn and W atom is in an approximately octahedral coordination surrounded by six nearest-

neighbor oxygen atom sites [11]. In addition to its relatively low melting point as well as desirable magnetic and multiferroic properties, the electrical conductivity of MnWO_4 is also sensitive to changes in humidity, thereby making it useful as a humidity sensor with potential applications ranging from medicine, meteorology, to agriculture [12].

Conventional preparatory methods for bulk MnWO_4 production are diverse, ranging from chemical reaction in molten salt media [13], mechanical grinding in a vibrating mill [14], to high-temperature decomposition of complex precursors [15]. Conversely, MnWO_4 nanocrystals have been synthesized by a solvothermal route, using an autoclave, in which hydrated MnCl_2 and Na_2WO_4 were annealed at 180°C in a pH range of 5–11 in the presence of homologous surfactants (such as ethylene glycol (EG), polyethylene glycol (PEG)-400, and PEG 10 000) [16]. Similarly, single-crystalline MnWO_4 nanoplates have been made by hydrothermally annealing hydrated MnSO_4 and Na_2WO_4 in the presence of DMF at 160°C for 10 days in an autoclave [17]. In addition, the sol-gel method has previously been used to generate MnWO_4 films [12].

Nonetheless, the motivation to generate one-dimensional (1D) nanostructures of these materials is high. Indeed, 1D nanostructures are fundamentally interesting because they are the lowest-dimensional anisotropic structures that can be used for the efficient transport of electrons and optical excitations [18,19]. Nanofibers and nanowires of MnWO_4 have primarily been fabricated by complexation-precipitation methods, associated with hydrothermal treatments of Na_2WO_4 and MnCl_2 (or MnSO_4) precursors either in the presence [11,16] or absence of [20]

* Corresponding author at: Department of Chemistry, State University of New York at Stony Brook, Stony Brook, NY 11794-3400, USA. Fax: +1631 632 7960, +1631 344 4071.

E-mail addresses: sswong@notes.cc.sunysb.edu, sswong@bnl.gov (S.S. Wong).

surfactant (such as cetyltrimethylammonium bromide, ethylene glycol, and polyethylene glycol) at temperatures ranging from 100 to 180 °C for periods of 4–24 h. All of these methods, however, necessitate a relatively high temperature of reaction (> 100 °C) as well as precise pH control in order to achieve the desired morphology.

In this manuscript, we have generalized a convenient, room temperature method, previously developed in the group for the synthesis of nanowires of BaWO₄, BaCrO₄, CaF₂, BaF₂, SrF₂, KMnF₃, and NH₄MnF₃ [21–24], in order to synthesize polycrystalline MnWO₄ nanowires and nanowire arrays through the mediation of a polycarbonate (PC) template. With this protocol, which operates under ambient conditions in aqueous solution with reliable control over shape, dimensionality, and crystallinity, we were able to make MnWO₄ nanowires and nanowire arrays under ambient conditions without the use of either surfactant or any high-temperature annealing treatment. Others have referred to this process as a precipitation metathesis reaction [25]. We also analyzed our MnWO₄ nanoscale samples using microscopy, spectroscopy, and magnetic measurements

2. Experimental

2.1. Synthesis

Commercially available PC membranes (Millipore Co. USA) used in this study possessed an average diameter of 50, 100 and 200 nm, respectively. These filter membranes contained track-etched channels with pores randomly distributed across their surface.

In a typical synthesis of MnWO₄ nanowires, a PC membrane was mounted between the two halves of a U-tube cell. The half-cells were then filled with 0.1 M solutions of Na₂WO₄ and MnCl₂ in water, respectively. After 12 h, the PC template was detached, thoroughly washed with distilled water, and ultimately removed by immersion in methylene chloride for 10 m. Isolated MnWO₄ nanowires were then obtained by initial centrifugation, followed by washing with ethanol and distilled water, and finally oven drying at 80 °C for 24 h. Bulk MnWO₄ samples were prepared in a similar way without the use of a template membrane. Specifically, 0.1 M aqueous solutions of Na₂WO₄ and MnCl₂ were mixed directly. The precipitates ultimately isolated were washed with distilled water and finally dried at 80 °C for 24 h.

2.2. Characterization

2.2.1. X-ray diffraction (XRD)

Crystallographic information on as-prepared samples was obtained using powder XRD through the mediation of a Scintag diffractometer, operating in the Bragg configuration using Cu K α radiation ($\lambda = 1.54 \text{ \AA}$). Tungstate samples for analyses were prepared by grinding powders thoroughly in ethanol using a mortar and pestle, followed by loading onto glass slides and subsequent drying in air. Diffraction patterns were collected from 15° to 65° at a scanning rate of 0.3° per minute with a step size of 0.02°. Parameters used for slit widths and accelerating voltages were identical for all samples.

2.2.2. Electron microscopy

The diameters and lengths of as-prepared tungstate nanowires were initially characterized using a field emission scanning electron microscopy instrument (FE-SEM Leo 1550), operating at an accelerating voltage of 15 kV and equipped with energy-dispersive X-ray spectroscopy (EDS) capabilities. Samples were

deposited onto double-sided conductive carbon tape, which was then ultimately attached onto the surfaces of SEM brass stubs. These samples were then conductively coated with gold by sputtering for 20 s, so as to minimize charging effects under SEM imaging conditions. For analysis of nanowire arrays, membranes were initially attached to a piece of conductive double-sided carbon tape. The resulting aligned samples were created by immersion in methylene chloride solution for 5 min in order to dissolve and remove the template. After washing with distilled water followed by air-drying, samples were subsequently mounted onto SEM brass stubs for imaging.

Specimens for transmission electron microscopy (TEM) and high-resolution TEM (HRTEM) were obtained by drying droplets of as-prepared samples from an ethanolic dispersion, which had been sonicated for 1 min, onto a 300 mesh Cu grid, coated with a lacey carbon film. TEM images were then taken at an accelerating voltage of 120 kV on a Philips CM12 instrument. HRTEM images were obtained using a JEOL 2010F HRTEM at an accelerating voltage of 200 kV.

2.2.3. Ultraviolet–visible spectra (UV–visible)

UV–visible spectra were obtained on a Thermospectronics UV1 spectrometer using quartz cells with a 10-mm path length. For these absorption spectral data, distilled water was used as a blank.

2.2.4. Infrared (IR) spectroscopy

Mid-IR spectra were recorded by using a Nicolet Nexus™ 470 FTIR spectrometer with a resolution of 4 cm⁻¹. Solid samples were prepared for analysis using a potassium bromide (KBr) pellet.

2.2.5. Squid

The field and temperature dependences of a bulk powder of MnWO₄ as well as a powder of MnWO₄ nanowires with an average diameter of 200 nm were measured. The experiments were carried out using a Quantum Designs Magnetic Phenomena Measurement System (MPMS) for temperatures ranging from 1.8 to 300 K, and in fields as large as 5 T. The nanoparticles were suspended in paraffin prior to measurement, and we have normalized their magnetization to that of the bulk powder at room temperature throughout. The bulk powder was compressed into a hard compact specimen weighing 0.009 g.

3. Results and discussion

The purity and crystallinity of as-prepared MnWO₄ samples were examined by powder XRD measurements (Fig. 1). All peaks can be readily indexed to a pure monoclinic phase (space group: *P2/c*) of MnWO₄ with calculated lattice constants of $a = 0.4813 \text{ nm}$, $b = 0.5783 \text{ nm}$, and $c = 0.5008 \text{ nm}$, which are in good agreement with database literature values ($a = 0.4829 \text{ nm}$, $b = 0.5759 \text{ nm}$, and $c = 0.4998 \text{ nm}$, JCPDS no. 13-0434, lower curve of Fig. 1).

The morphology of as-synthesized one-dimensional samples, derived from a 200 nm PC template, was studied using FE-SEM and TEM. Fig. 2 shows SEM images of as-prepared MnWO₄ nanowires, isolated from a PC template, possessing 200 nm pore sizes. Diameters of MnWO₄ nanowires were noted to be $\sim 260 \pm 40 \text{ nm}$, whereas their associated lengths measured $\sim 5.4 \pm 1.2 \mu\text{m}$. Fig. 2B (top view) and 2C (tilt view) show images of as-generated MnWO₄ arrays upon removal of the PC template. The EDS spectrum (Fig. 2D) confirms the existence of Mn, W, and O, as expected. Sample morphology of the samples was also characterized using low-magnification TEM as shown in Fig. 3A. These images further confirm the dimensional range of as-

prepared nanowires, calculated from SEM data. It should also be mentioned that as-obtained nanowires were noted to be relatively uniform in terms of shape and morphology. A HRTEM image (Fig. 3B) and associated FFT image (inset to Fig. 3B) taken on an individual MnWO_4 nanowire show the polycrystalline nature of the sample. The lattice spacing measured in the image can be indexed to the (-111) plane. Additional SEM images of MnWO_4 nanowires, prepared using templates with pore diameters measuring 50 and 100 nm, respectively, are presented in Fig. 4. The diameters of these particular MnWO_4 nanowires are 55 ± 10 and 100 ± 20 nm, respectively, consistent with the pore size dimensions of the originating templates themselves with associated lengths of 2.0 ± 0.5 and $3.0 \pm 1.1 \mu\text{m}$, respectively. The morphology of bulk samples was also investigated using FE-SEM

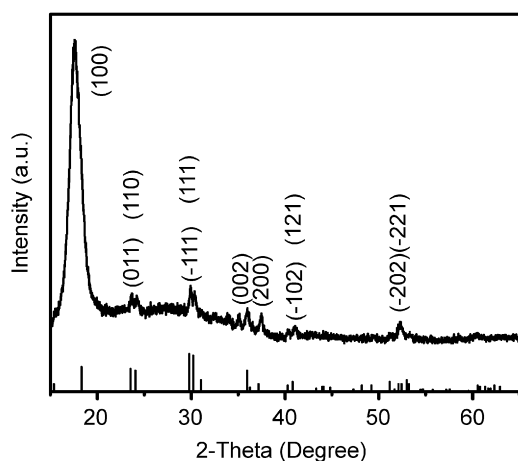


Fig. 1. XRD patterns of as-prepared samples (upper half) and of the corresponding database standard (JCPDS #13-0434, lower half).

as shown in Fig. 5. The bulk samples essentially consisted of uniform particulate structures with diameters in the range of $1.5 \pm 0.1 \mu\text{m}$. EDS patterns showed the presence of peaks associated with Mn, W and O, respectively.

Optical properties of as-prepared 200 nm nanowire samples were also investigated from the UV to IR range. The IR spectrum (Fig. 6A) of MnWO_4 nanowires shows a number of absorption bands (located at 579, 669, 757, 810, 875, and 912 cm^{-1}) in the range of $500\text{--}1000 \text{ cm}^{-1}$ which are similar to that of the bulk IR pattern previously reported for $\text{MnWO}_4 \cdot \text{H}_2\text{O}$, wherein the inorganic modes lie at the low-wavenumber end of the spectra [26]. Many of these infrared bands can be assigned to internal stretching modes, i.e. $\nu_3(A_u)$ and $\nu_3(E_u)$ transitions [27]. The UV–visible (Fig. 6B) spectrum showed a similarity in the absorption profile between that of the 200 nm nanowires and of the bulk.

The magnetic behavior of our as-prepared 200 nm MnWO_4 nanowires was investigated using SQUID analysis. MnWO_4 has been considered as a moderately frustrated antiferromagnetic spin system [8]. Bulk MnWO_4 has been found to undergo successive magnetic phase transitions at $\sim 13.5 \text{ K}$ (T_N), $\sim 12.7 \text{ K}$ (T_2), and $\sim 7.6 \text{ K}$ (T_1), corresponding to three long-wavelength magnetic ordering states: AF3, AF2, and AF1 [6,28]. The ground state, AF1 ($T < T_1$), is a commensurate collinear antiferromagnetic phase; the magnetic moments are aligned collinearly along the ‘easy’ axis of magnetization, which is within the ac plane at an angle of $35\text{--}37^\circ$ from the a -axis. By contrast, AF2 ($T_1 < T < T_2$) consists of an incommensurate elliptically modulated spiral spin structure. Finally, the AF3 ($T_2 < T < T_N$) phase denotes an incommensurate, sinusoidal collinear AFM structure with magnetic moments lying along the x -axis [6,8]. Prior investigations of the magnetic properties of MnWO_4 were mainly performed on bulk samples so it was important to note the comparable behavior of MnWO_4 nanowires.

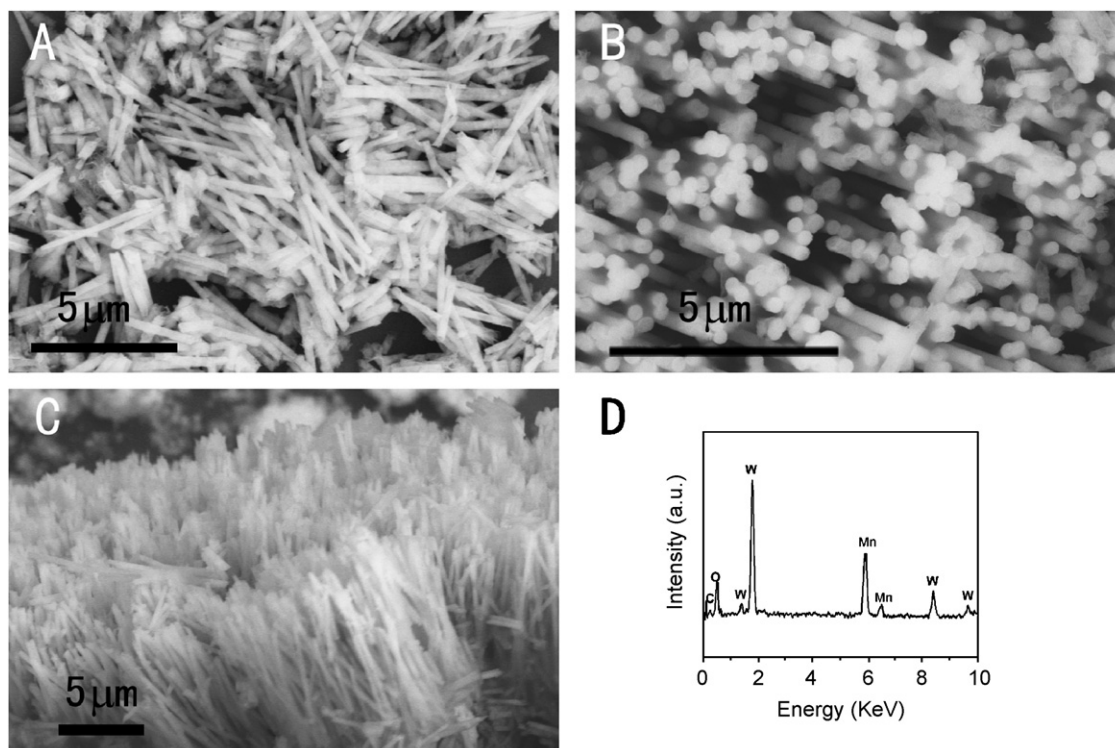


Fig. 2. SEM images of (A) isolated MnWO_4 nanowires, (B) MnWO_4 arrays (top view), (C) MnWO_4 arrays (side view) and (D) Representative EDS pattern of as-prepared MnWO_4 nanowires and nanowire arrays.

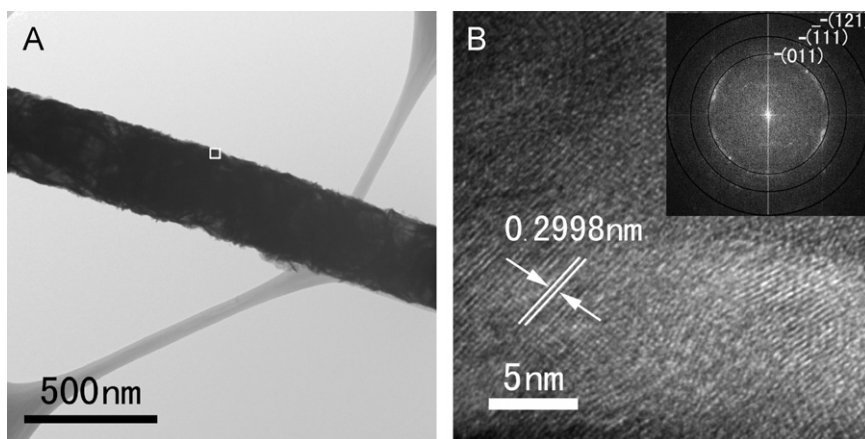


Fig. 3. TEM (A) and HRTEM (B) images as well as the corresponding FFT pattern (inset) of MnWO_4 nanowires.

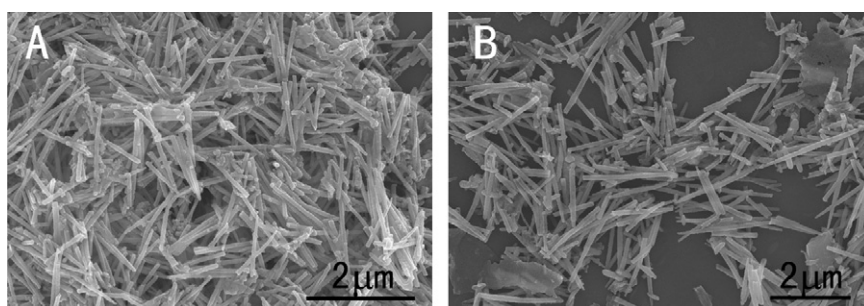


Fig. 4. SEM images of isolated MnWO_4 nanowires prepared from (A) a $50\ \mu\text{m}$ PC template and (B) a $100\ \mu\text{m}$ PC template.

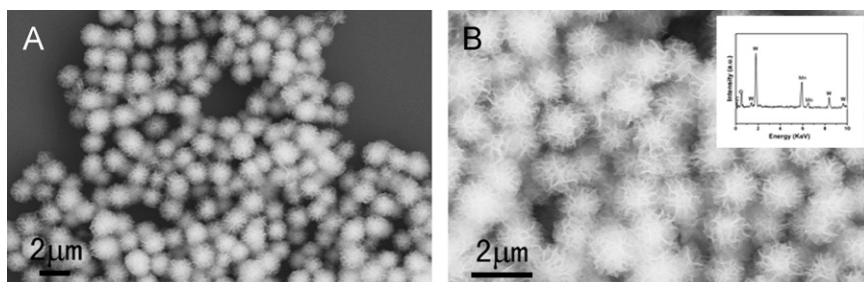


Fig. 5. SEM images as well as an EDS pattern (inset to B) of bulk MnWO_4 .

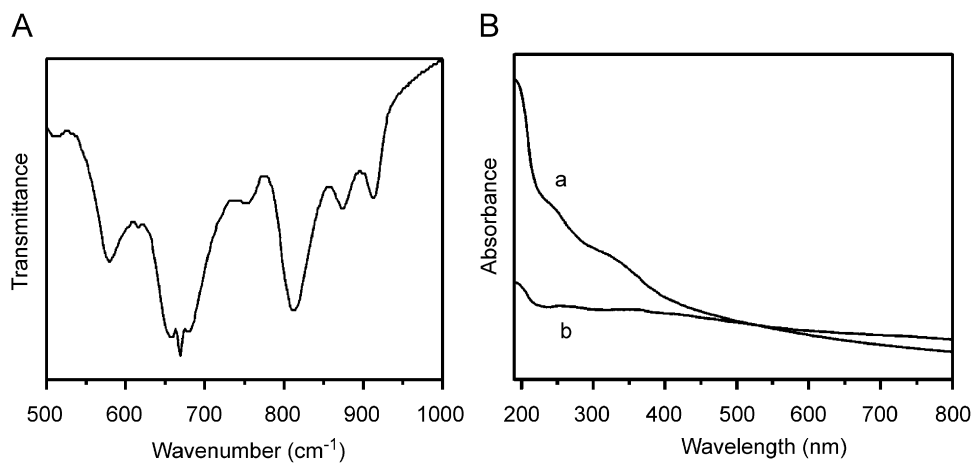


Fig. 6. IR spectrum (A) and UV-visible spectrum (B) of MnWO_4 ((a) bulk and (b) nanowires).

The temperature dependence of the magnetic susceptibility, measured in a field of 0.1 T, has been compared for the two samples in Fig. 7A and B, measured after cooling in zero field (ZFC) and in a field of 5 T (FC). In all cases, the susceptibility increases with decreasing temperature, reaching a single broad maximum near 7 K. Fig. 8 shows that the susceptibility is well described by the Curie–Weiss law for temperatures from 10 to 300 K, indicating that it arises from a conventional paramagnetic state involving independent fluctuations of independent Mn moments. The Weiss temperature, $\theta = -25$ K, implies a net antiferromagnetic interaction among the Mn moments, with a magnitude in reasonable agreement with the value of $\theta = -15$ K found for bulk powdered MnWO_4 .

The maximum in the susceptibility signals the onset of magnetic order at ~ 7.5 K, presumably antiferromagnetic order, although the breadth of the maximum and also the separation of the FC and ZFC data below this ordering temperature suggests an appreciable level of magnetic frustration and perhaps short range order. In principle, this might result in the nanoparticle samples experiencing a superparamagnetic effect caused by uncompensated surface moments. However, the results found for the bulk powder are very similar and we conclude that disorder is a more likely explanation. That is, while the presence of chemical impurity might normally account for the slight anomaly observed, we did not detect any such magnetic impurity in our samples. Hence, these observations can potentially be assigned to structural disorder in the sample, such as the presence of small-crystalline particulate regions, an assertion supported by the polycrystalline nature of our metal tungstate nanowires, as evidenced by the TEM/HRTEM images in Fig. 3A and B. Indeed, the susceptibility peak in both of our samples is much broader and occurs at a lower temperature than that previously reported for a MnWO_4 powder [10] and a single crystal [6]. What is more, no features are found in the temperature derivative of the susceptibility, which might correspond to the three thermodynamic transitions found in heat capacity measurements [10].

The field dependences of the magnetization for both the bulk and nanoparticle samples are presented in Fig. 9A and B. The magnetization is always linear in field, showing that the magnetic response is dominated by that of the individual moments, both above and below the antiferromagnetic ordering temperature. The rapid reduction in the slope of the magnetization curves with increased temperature is wholly congruent with the overall Curie–Weiss susceptibility. Accordingly, we have plotted the ZFC susceptibility data, $\chi = M/H$, measured for both samples as a function of H/T in Fig. 10, to confirm that the magnetization

sweeps taken at temperatures from 3 to 80 K all collapse onto universal curves, presumed to be approximated by Brillouin functions. This collapse shows that the magnetization is dominated by fluctuations of individual Mn moments, and not by critical fluctuations or other collective effects.

Taken together, these magnetic measurements reveal a system in which antiferromagnetic short-range order is established, although the development of these correlations is sluggish and coexists with a predominantly paramagnetic response both above and below the transition. No evidence for finite size effects due to particle size was found in these nanowire samples, which show almost the same properties as that of the bulk powder of MnWO_4 .

3.1. Plausible formation mechanism

As described previously in other papers [21–24], in the current experiment, we use the pores of PC membranes as the physical environment in which to control the growth of well-defined morphologies of crystals of our manganese tungstate structures. The membranes used are thin, and are mounted in a double-diffusion setup, which enables the continuous flow of ions into the membrane pores but prevents their overly rapid mixing. Thus, in the experimental setup used in these experiments, the contents of each solution in either half of the U-tube are allowed to diffuse towards each other across a wetted template membrane

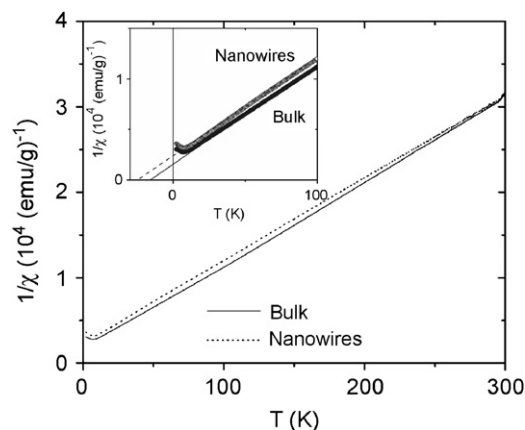


Fig. 8. Temperature dependence of the inverse susceptibility χ^{-1} for bulk (solid line) and 200 nm nanowire (dashed line) samples. Inset compares linear fits (solid line (bulk), dashed line (nanowires)), indicating that the Curie–Weiss law is valid for temperatures from ~ 15 to 300 K.

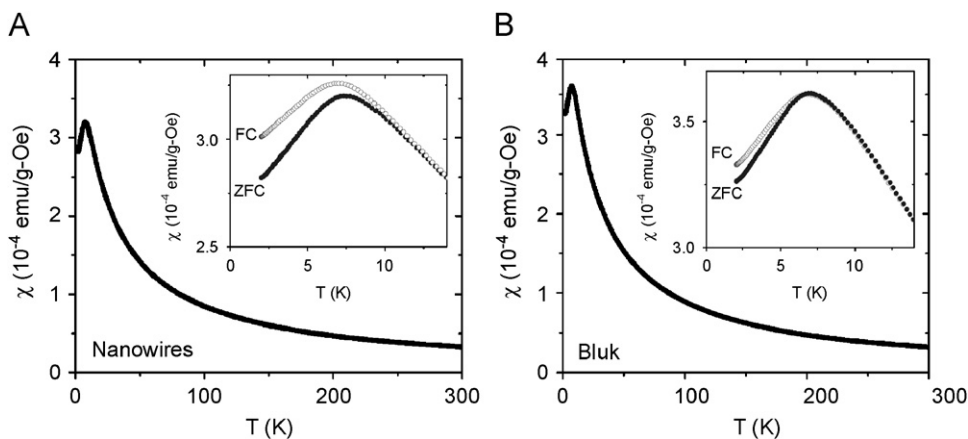


Fig. 7. (A) Magnetic susceptibility χ of powder of 200 nm nanowires, measured in a field of 0.1 T. The inset shows a modest hysteresis between data taken under zero field cooled (ZFC) and data taken after cooling in a 5 T field (FC). (B) Same, but for a bulk powder sample of MnWO_4 .

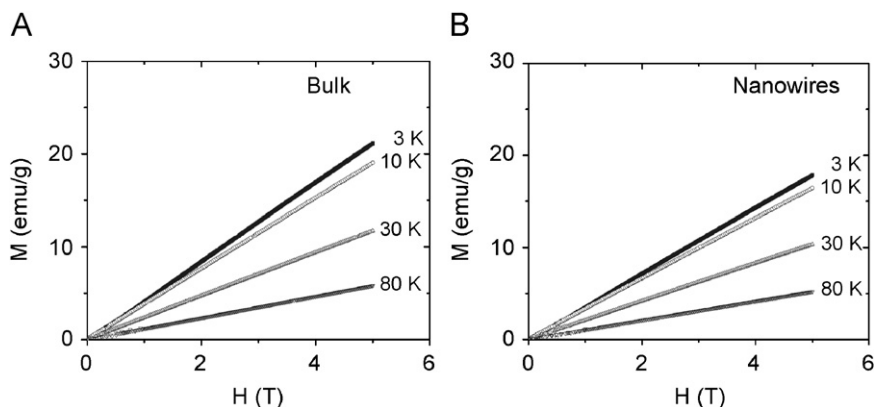


Fig. 9. Field dependences of the magnetization M , at different fixed temperatures for the bulk MnWO_4 powder (A) and 200 nm nanowires (B).

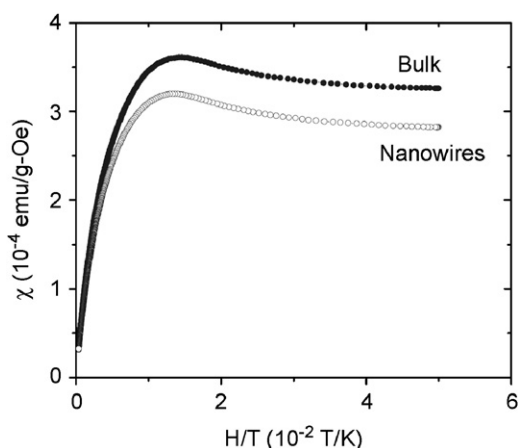


Fig. 10. Field-temperature scaling behavior of the susceptibility $\chi = M/H$ is measured for both the bulk powder and the 200 nm nanowire samples.

physically separating the two halves. Manganese cations and tungstate anions meet at the interface, react in a precipitation/metathesis process, and nucleate the formation of the corresponding metal tungstates. These insoluble tungstates will begin to precipitate from solution, once the supersaturation value for their production has been exceeded.

If the interactions between reagent molecules are stronger than those between the reagent molecules and the pore walls, the nucleation process and accompanying product formation will tend to happen within the voluminous confines of the pores themselves in a homogeneous-type process. That is, crystals of nanoscale metal tungstates therefore derive from isolated, disparate nucleation sites, which then grow by extension throughout the porous network. Continued growth then occurs at the particle surface at a rate limited by ion availability, until the crystal impinges upon the relatively inert template surface itself, which ultimately limits further particle growth. Within the cylindrical confines of the template pores, as-formed particles in this scenario essentially self-assemble with each other into either wire-like or rod-like motifs.

Conversely, if the interactions between the reagent molecules are weaker than those between the reagent molecules and the pore walls, the nucleation and accompanying growth processes may tend to be localized at the surfaces of the pore walls in a heterogeneous-type process. Such a process may occur, for instance, if the pore wall is positively charged while the reagent particles are negatively charged. This preferential confinement of growth to the inherent geometry of the pore walls can therefore

lead to the generation of primarily tube-like motifs upon the elongation and assembly of the as-formed particles. With continued reaction, nanowire formation can be viewed as a lateral thickening of the tubular structure, which, as further supply of precursors to the inside is blocked by the ever-growing tube thickness coupled with an ever-decreasing inner tube diameter, eventually constricts the entire porous interior of the template, filling it completely. In other words, continued growth of the nanotubes is limited only by reagent ion availability and diffusivity as well as by intrinsic geometrical constraints imposed by the template channels. Hence, nanowires can be considered as the ultimate limit of nanotube growth, at least in terms of its width.

4. Conclusions

MnWO_4 nanowires and nanowire arrays have been synthesized by a simple, room-temperature method with the aid of a PC template. These reactions have been run under simplistic, ambient conditions in aqueous solutions with reproducibility in terms of morphology and chemical composition. We have also used this protocol not only to generate isolated structures but also to produce arrays of these ternary metal oxides. As-synthesized nanowires measured 260 ± 40 nm in diameter and 5.4 ± 1.2 μm in length, isolated from a 200 nm PC template. Those generated from templates with pore diameters of 50 and 100 nm measured 55 ± 10 and 100 ± 20 nm, respectively, with accompanying lengths in the microns. Optical and magnetic properties of MnWO_4 nanowires have been investigated, suggestive of subtle differences in behavior between bulk and nanoscale manifestations of an identical material. The fact that the nanowires were polycrystalline did not obviously appear to adversely affect the performance metrics of these materials. However, it is obvious that for many systems, the ability to generate pure, single-crystalline motifs is crucial to relevant structure–property correlations. Hence, in terms of future work, we will likely explore other methods of nanoscale MnWO_4 preparation, including using catanionic reverse micelles [29–32].

Acknowledgments

We acknowledge the US Department of Energy (DE-AC02-98CH10886) for facility and personnel support. We also thank the National Science Foundation (CAREER Award DWR-0348239), and the Alfred P. Sloan Foundation for PI support and experimental supplies. Moreover, we are grateful to D. Wang (Boston College) as

well as to S. van Horn and J. Quinn (SUNY Stony Brook) for their assistance with electron microscopy.

Appendix A. Supplementary Materials

Supplementary data associated with this article can be found in the online version at doi:10.1016/j.jssc.2008.03.009.

References

- [1] R. Ramesh, N.A. Spaldin, *Nat. Mater.* 6 (2007) 21.
- [2] T. Kimura, T. Goto, H. Shintani, K. Ishizaka, T. Arima, Y. Tokura, *Nature* 426 (2003) 55.
- [3] J. Wang, J.B. Neaton, H. Zheng, V. Nagarajan, S.B. Ogale, B. Liu, D. Viehland, V. Vaithyanathan, D.G. Schlom, U.V. Waghmare, N.A. Spaldin, K.M. Rabe, M. Wuttig, R. Ramesh, *Science* 299 (2003) 1719.
- [4] T. Kimura, S. Kawamoto, I. Yamada, M. Azuma, M. Takano, Y. Tokura, *Phys. Rev. B* 67 (2003), 180401-1.
- [5] R. Feyerherm, E. Dudzik, N. Aliouane, D.N. Argyriou, *Phys. Rev. B* 73 (2006), 180401-1.
- [6] K. Taniguchi, N. Abe, T. Takenobu, Y. Iwasa, T. Arima, *Phys. Rev. Lett.* 97 (2006) 097201–097203.
- [7] H. Ehrenberg, H. Weitzel, C. Heid, H. Fuess, G. Wltschek, T. Kroener, J.V. Tol, M. Bonnet, *J. Phys.: Condens. Matter* 9 (1997) 3189.
- [8] A.H. Arkenbout, T.T.M. Palstra, T. Siegrist, T. Kimura, *Phys. Rev. B* 74 (2006), 184431-1.
- [9] O. Heyer, N. Hollmann, I. Klassen, S. Jodlauk, L. Bohatý, P. Becker, J.A. Mydosh, T. Lorenz, D. Khomskii, *J. Phys.: Condens. Matter* 18 (2006) L471.
- [10] G. Lautenschläger, H. Weitzel, T. Vogt, R. Hock, A. Böhm, M. Bonnet, H. Fuess, *Phys. Rev. B* 48 (1993) 6087.
- [11] S. Lei, K. Tang, Z. Fang, Y. Huang, H. Zheng, *Nanotechnology* 16 (2005) 2407.
- [12] W. Qu, W. Wlodarski, J.-U. Meyer, *Sensors Actuators B* 64 (2000) 76.
- [13] V.D. Schultze, K.T. Wilke, C. Waligora, *Anorg. Allg. Chem.* 352 (1967) 184.
- [14] V.R. Alvrecht, R. Möbius, *Anorg. Allg. Chem.* 392 (1972) 62.
- [15] M. Jang, T.J.R. Weakley, K.M. Doxsee, *Chem. Mater.* 13 (2001) 519.
- [16] S.-J. Chen, X.-T. Chen, Z. Xue, J.-H. Zhou, J. Li, J.-M. Hong, X.-Z. You, *J. Mater. Chem.* 13 (2003) 1132.
- [17] L. Zhang, C. Lu, Y. Wang, Y. Cheng, *Mater. Chem. Phys.* 103 (2007) 433.
- [18] Y. Xia, P. Yang, Y. Sun, Y. Wu, B. Mayers, B. Gates, Y. Yin, F. Kim, H. Yan, *Adv. Mater.* 15 (2003) 353.
- [19] G.R. Patzke, F. Krumeich, R. Nesper, *Angew. Chem. Int. Ed. Engl.* 41 (2002) 2446.
- [20] S.-H. Yu, B. Liu, M.-S. Mo, J.-H. Huang, X.-M. Liu, Y.-T. Qian, *Adv. Funct. Mater.* 13 (2003) 639.
- [21] Y. Mao, S.S. Wong, *J. Am. Chem. Soc.* 126 (2004) 15245.
- [22] Y. Mao, F. Zhang, S.S. Wong, *Adv. Mater.* 18 (2006) 1895.
- [23] Y. Mao, T.-J. Park, F. Zhang, H. Zhou, S.S. Wong, *Small* 3 (2007) 1122.
- [24] F. Zhang, Y. Mao, T.-J. Park, S.S. Wong, *Adv. Funct. Mater.* 18 (2008) 112.
- [25] J.-S. Jung, L. Ren, C.J. O'Connor, *J. Mater. Chem.* 2 (1992) 829.
- [26] B. Ingham, S.V. Chong, J.L. Tallon, *Curr. Appl. Phys.* 6 (2006) 553.
- [27] P. Tarte, M. Liegeois-Duyckaerts, *Spectrochim. Acta—Part A* 28A (1972) 2029.
- [28] H. Ehrenberg, H. Weitzel, H. Fuess, *Physica B* 234–236 (1997) 560.
- [29] H. Shi, L. Qi, J. Ma, H. Cheng, *J. Am. Chem. Soc.* 125 (2003) 3450.
- [30] H. Shi, L. Qi, J. Ma, H. Cheng, B. Zhu, *Adv. Mater.* 15 (2003) 1647.
- [31] H. Shi, L. Qi, J. Ma, N. Wu, *Adv. Funct. Mater.* 15 (2005) 442.
- [32] H. Shi, X. Wang, N. Zhao, L. Qi, J. Ma, *J. Phys. Chem. B* 110 (2006) 748.